

Hydrothermal preparation and characterization of ZnFe_2O_4 magnetic nanoparticles as an efficient heterogeneous catalyst for the synthesis of multi-substituted imidazoles and study of their anti-inflammatory activity

Adel A. Marzouk¹ | Ahmed M. Abu-Dief²  | Antar A. Abdelhamid²

¹Pharmaceutical Chemistry Department, Faculty of Pharmacy, Al Azhar University, Egypt

²Department of Chemistry, Faculty of Science, Sohag University, 82524 Sohag, Egypt

Correspondence

Ahmed M. Abu-Dief, Department of Chemistry, Faculty of Science, Sohag University, 82524 Sohag, Egypt.

Email: ahmed_benzoic@yahoo.com

Nanoparticles are key focus of research for a wide range of novel applications. As such, ZnFe_2O_4 magnetic nanoparticles were synthesized hydrothermally and characterized via scanning and transmission electron microscopies, powder X-ray diffraction, energy-dispersive X-ray and infrared spectroscopies, thermogravimetric analysis and magnetic measurements. They were used as a robust catalyst for the synthesis of a series of biologically active multi-substituted imidazoles using a multicomponent reaction by the reaction of benzil with various aromatic aldehydes, ammonium acetate and aliphatic amines (*N,N*-dimethyl-1,3-propanediamine and 1-amino-2-propanol) under solvent-free conditions. The key advantages of this method are shorter reaction times, very high yield and ease of operation. The thermally and chemically stable, benign and economical catalyst was easily recovered using an external magnet and reused in at least five successive runs without an appreciable loss of activity. All of these novel synthesized compounds were characterized from spectral data and their purities were checked using thin-layer chromatography, giving one spot. Furthermore, the prepared compounds were tested for their anti-inflammatory activity.

KEYWORDS

biologically active, efficient catalyst, imidazoles, multicomponent reaction, non-chromatographic method, superparamagnetic materials, ZnFe_2O_4 nanoparticles

1 | INTRODUCTION

One of the potential applications of nanoparticles seems to be as catalysts for the development of new synthetic methods for organic transformations in environmentally benign processes.^[1–4] Among nanoparticles, magnetite nanoparticles have attracted much attention due to their uses in the synthesis of ferro fluids, as magnetic resonance imaging agents for the diagnosis of many diseases and also as catalysts in organic transformations.^[5–7] These kinds of catalysts can be recovered and separated from reaction mixtures using an external or internal magnet which is simpler and more

efficient than filtration or centrifugation. Most recently, Fe_3O_4 nanoparticles have been used extensively as a heterogeneous magnetic nanoparticle support for catalysts in organic transformations.^[8,9]

The imidazole ring is one of the most important structures in the field of heterocyclic chemistry. In the last few decades, many publications have shown the widespread biological activity of imidazole derivatives, such as anticonvulsant, anticancer and antimicrobial activities. Especially for antifungal activity, dozens of imidazole derivatives have been developed as commercial fungicides.^[10,11] Imidazoles are important heterocycles occurring in natural compounds,

antifungal drugs and many other artificial substances with a variety of other biological activities, applicable in medicinal chemistry and pharmacology, as well as in material science, catalysis and the preparation of ionic liquids. Numerous methods for the synthesis of imidazoles have been designed, and several pertinent reviews have appeared. Recently, a photochemical one-pot three-component synthesis of tetra-substituted imidazoles has been reported.^[12–18]

Multicomponent reactions are a distinctive class of synthetic organic processes that create complex compounds from the reaction of three or more simple starting materials in one pot. Because of the operational smoothness, atom-economy and structural diversity and complexity of the molecules that can be prepared in these reactions, they have attracted much attention. Multicomponent reactions have an increasing importance in medicinal and organic chemistry due to their various applications in diversity-oriented convergent preparations of complex organometallic molecules from simple and readily available substrates in a single vessel.^[19]

In the work reported here, we developed the one-step construction of an extensive series of imidazole derivatives by the combination of benzil with various aldehydes, ammonium acetate and 1-amino-2-propanol in the presence of ZnFe₂O₄ magnetic nanoparticles. The reaction is complete after a few minutes of refluxing. The process represents a significant improvement over existing methods of imidazole synthesis.

2 | EXPERIMENTAL

2.1 | Materials

All reagents used in the investigation were of analytical grade and used without further purification. Fe(NO₃)₃·9H₂O (Sigma-Aldrich) and Zn(NO₃)₂·6H₂O (Sigma-Aldrich) served as iron and zinc precursors, while NaOH (pellets, 98%, Alfa Aesar) was the precipitating agent and poly(ethylene glycol) 400 (PEG-400; Sigma-Aldrich) was used as a surfactant. All solutions were prepared with distilled water.

2.2 | Synthesis of ZnFe₂O₄ nanoparticles

ZnFe₂O₄ nanoparticles were prepared using stoichiometric molar amounts of ferric nitrate Fe(NO₃)₃·9H₂O and zinc nitrate Zn(NO₃)₂·6H₂O which were dissolved in 30 ml of water and stirred magnetically until complete solubility of the reactants. Then, 5 ml of PEG-400 was added dropwise to the mixture to serve as a surfactant that covers the nanoparticles and prevents agglomeration. The resulting solution was stirred for an addition 1 h. After that, the pH was adjusted to 12 by adding NaOH (2 M) dropwise. After 2 h under continuous stirring, a homogeneous solution containing hydroxide precipitates of the precursors was obtained. Finally, the resulting reaction mixture (total volume of 75 ml) was sealed

in a Teflon-lined stainless autoclave, heated at 180 °C in a Memmert GmbH furnace for 20 h, and then cooled to room temperature gradually. The obtained products were centrifuged, washed several times with deionized water, acetone and absolute ethanol, and then dried at 90 °C for 2 h. The sample was gently ground in an agate mortar to reduce the required orientation.^[3,4]

2.3 | Instrumentation

A HANNA 211 pH meter was used to measure the pH values. Powder X-ray diffraction (PXRD) patterns were recorded using a PANalytical X'Pert PRO diffractometer with Cu K_α radiation (1.5418 Å). All data were gathered at room temperature over the angular range of $2\theta = 10\text{--}80^\circ$ with a step of 0.05° and a counting time of 2.5 s per step. The instrumental resolution was determined using LaB6 standard reference material (SRM 660a) provided by National Institute of Standards and Technology (NIST), which is usually used for calibrating line position and line shape in powder diffractometers. Scanning electron microscopy (SEM) and X-ray microanalysis were conducted with a JEOL 6610VL microscope operating at 20 kV equipped with an X-Max silicon drift detector for energy-dispersive X-ray spectroscopy (EDS) analysis. Transmission electron microscopy (TEM) studies were performed with a JEOL JEM-2100F microscope operated at an accelerating voltage of 200 kV, equipped with a field emission gun and an ultrahigh-resolution pole-piece that provided a point resolution better than 0.19 nm. The prepared ZnFe₂O₄ nanoparticles for TEM observation were dispersed in ethanol, sonicated and sprayed on a carbon-coated copper grid and then left to air-dry. Finally, a Gatan SOLARUS 950 was used before observation. Particle size distribution of the nanoparticles was determined using Image J Launcher, broken-symmetry software, version (1.4.3.6.7).^[20] The magnetic properties of the prepared nanoparticles were determined using a Quantum Design Physical Property Measurement System with vibrating sample magnetometry (VSM) option. For magnetic measurements, dried powder specimens were compacted and encapsulated into polypropylene powder holders that snap onto the commercial brass trough for a secure press fit. Then, magnetization (M) as a function of temperature (T) was measured under an applied magnetic field (H) of 100 Oe at 5 and 300 K.

2.4 | General procedure for preparation of multi-substituted imidazoles (5a–n) catalysed by ZnFe₂O₄ nanoparticles

2.4.1 | Materials and instrumentation

All commercially available reagents were purchased from Merck, Aldrich and Fluka. All reactions were checked by

TLC using percolated plates of silica gel G/UV-254 of 0.25 mm thickness (Merck 60F254) using UV light (254/365 nm) for visualization. Melting points were measured with a Kofler melting points apparatus and were uncorrected. Fourier transform infrared (FT-IR) spectra were recorded with a Bruker FT-IR-ALPHA Platinum-ATR. ^1H NMR and ^{13}C NMR spectra were recorded in deuterated dimethylsulfoxide (DMSO- d_6) with a Bruker Bio Spin AG spectrometer at 400 and 100 MHz, respectively. For ^1H NMR, chemical shifts (δ) were measured in ppm with reference to tetramethylsilane (TMS) as an internal standard ($\delta = 0$ ppm); coupling constants (J) were measured in hertz (Hz) and data are reported as follows: chemical shift, integration, multiplicity (s = singlet, d = doublet, t = triplet, q = quartet, m = multiplet). For ^{13}C NMR, TMS ($\delta = 0$ ppm) or DMSO ($\delta = 39.51$ ppm) was used as internal standard and spectra were obtained with complete proton decoupling. Elemental analyses were conducted with a PerkinElmer CHN analyser.

2.4.2 | Procedures

Amounts of 0.02 mol of aromatic aldehyde, 0.02 mol of benzil, 0.02 mol of ammonium acetate and 0.02 mol of aliphatic amine (*N,N*-dimethyl-1,3-propanediamine or 1-amino-2-propanol) were added to 20 ml of absolute ethanol and ZnFe_2O_4 nanoparticles (5 mmol%). The reaction mixture was stirred for 30–50 min. Then, the reaction mixture was continued stirring for the specified time. The completion of the reaction was determined by TLC. The catalyst was separated magnetically and the reaction mixture was filtered and the solid product was crystallized from an appropriate solvent to afford the pure products. The pure products were obtained without using any chromatographic techniques, simply by recrystallization from ethanol. FT-IR and NMR data for the prepared compounds are shown in Figures S1–S14 and listed below.

2-(1-(2-hydroxypropyl)-4,5-diphenyl-1H-imidazol-2-yl)phenol (5a)

M.p. 80–82 °C. FT-IR (KBr, cm^{-1}): 3410 (OH), 3060, 3033 (C–H), 2969, 2928 (C–H), 2840, 1596 (C=N) 1550 (C=C), 1484, 1448, 1375, 1293, 1211, 1175, 1073, 874, 757, 697, 643. ^1H NMR (DMSO- d_6 /D $_2$ O, 300 MHz): 0.71 (d., 3H, CH_3 –CH), 3.47 (d., 2H, CH_2N), 3.87 (m., 1H, CH_2 – $\text{CH}(\text{OH})$ – CH_3), 4.91 (s. br., 1H, CH_2 – $\text{CH}(\text{OH})$ – CH_3), 6.95–7.95 (m., 14H, Ar-H), 11.10 (s.br., 1H, Ar-OH). ^{13}C NMR (300 MHz, DMSO- d_6): 21.25, 52.16, 64.98, 116.83, 116.97, 119.44, 126.49, 126.66, 128.59, 129.29, 129.46, 129.53, 129.97, 130.05, 130.22, 130.33, 130.75, 131.40, 131.68, 134.80, 135.89, 135.99, 145.73, 156.39, 156.50. DEPT 135 (300 MHz, DMSO- d_6): 52.16 (CH_2) ppm disappeared.

2-(1-(4-hydroxypropyl)-4,5-diphenyl-1H-imidazol-2-yl)phenol (5b)

M.p. 212–214 °C. FT-IR (KBr, cm^{-1}): 3255 (OH), 3060 (C–H), 2955 (C–H), 2845, 1616 (C=N) 1540 (C=C), 1483, 1399, 1288, 1118, 835, 697, 619, 539. ^1H NMR (DMSO- d_6 /D $_2$ O, 300 MHz): 0.67 (d., 3H, CH_3 –CH), 3.35 (d., 2H, CH_2N), 3.83 (m., 1H, CH_2 – $\text{CH}(\text{OH})$ – CH_3), 4.87 (s. br., 1H, CH_2 – $\text{CH}(\text{OH})$ – CH_3), 6.91–7.64 (m., 14H, Ar-H), 11.10 (s.br., 1H, Ar-OH). ^{13}C NMR (300 MHz, DMSO- d_6): 21.29, 51.85, 64.85, 115.79, 122.62, 126.41, 126.67, 128.45, 129.08, 129.46, 129.92, 131.10, 131.51, 131.90, 135.39, 136.59, 148.26, 158.43. DEPT 135 (100 MHz, DMSO- d_6): 51.85 (CH_2) ppm disappeared.

1-(2-(4-fluorophenyl)-4,5-diphenyl-1H-imidazol-1-yl)propan-2-ol (5c)

M.p. 170–172 °C. FT-IR (KBr, cm^{-1}): 3148 (OH), 3077 (C–H), 2988 (C–H), 2959, 2924, 1605 (C=N) 1529 (C=C), 1481, 1423, 1334, 1230, 1134, 1074, 849, 821, 774, 697. ^1H NMR (DMSO- d_6 /D $_2$ O, 300 MHz): 0.69 (d., 3H, CH_3 –CH), 3.39 (d., 2H, CH_2N), 3.87 (m., 1H, CH_2 – $\text{CH}(\text{OH})$ – CH_3), 4.98 (s. br., 1H, CH_2 – $\text{CH}(\text{OH})$ – CH_3), 7.12–7.93 (m., 14H, Ar-H). ^{13}C NMR (100 MHz, DMSO- d_6): 21.31, 51.97, 64.96, 115.77, 115.98, 126.56, 126.67, 128.49, 129.24, 129.51, 130.41, 131.50, 131.68, 131.91, 131.99, 135.20, 137.00, 147.00, 161.52, 163.97. DEPT 135 (100 MHz, DMSO- d_6): 51.97 (CH_2) ppm disappeared.

1-(2-(4-isopropylphenyl)-4,5-diphenyl-1H-imidazol-1-yl)propan-2-ol (5d)

M.p. 198–220 °C. FT-IR (KBr, cm^{-1}): 3370 (OH), 3054 (C–H), 2962 (C–H), 2927, 2870, 1603 (C=N) 1520 (C=C), 1483, 1337, 1023, 969, 937, 842, 773, 697, 561. ^1H NMR (DMSO- d_6 /D $_2$ O, 300 MHz): 0.67 (d., 3H, CH_3 –CH), 1.27 (d., 3H, $(\text{CH}_3)_2$ –CH), 2.98 (m., 1H, $(\text{CH}_3)_2$ –CH), 3.38 (d., 2H, CH_2N), 3.88 (m., 1H, CH_2 – $\text{CH}(\text{OH})$ – CH_3), 4.90 (s. br., 1H, CH_2 – $\text{CH}(\text{OH})$ – CH_3), 7.12–7.76 (m., 14H, Ar-H). ^{13}C NMR (300 MHz, DMSO- d_6): 21.25, 22.51, 24.24, 51.90, 64.83, 126.47, 126.59, 126.83, 126.93, 127.62, 128.46, 129.17, 129.50, 129.62, 131.48, 135.38, 138.84, 147.50, 148.22. DEPT 135 (100 MHz, DMSO- d_6): 51.90 (CH_2) ppm disappeared.

3-(2-(2-methoxyphenyl)-4,5-diphenyl-1H-imidazol-1-yl)-*N,N*-dimethylpropan-1-amine (5e)

M.p. 121–123 °C; yield 92%. FT-IR (KBr, cm^{-1}): 3060 (C–H) aromatic, 2944–2722 (C–H) aliphatic, 1603 (C=N). ^1H NMR (DMSO- d_6 /D $_2$ O, 300 MHz): 1.30–1.35 (m., 2H, CH_2 – CH_2 – CH_2), 1.75 (s., 6H, $(\text{CH}_3)_2\text{N}$), 1.82 (t., 2H, $(\text{CH}_3)_2\text{NCH}_2$ – CH_2 – CH_2 –N), 3.67 (t, 2H, $(\text{CH}_3)_2\text{NCH}_2$ – CH_2 – CH_2 –N), 3.7 (s., 3H, OCH_3) 7.11–

7.53 (m., 14H, Ar-H). ^{13}C NMR (100 MHz, DMSO- d_6 /D $_2$ O): 28.17, 42.83, 44.97, 56.02, 56.49, 112.14, 121.01, 126.32, 126.44, 128.39, 129.15, 129.57, 131.42, 131.81, 132.60, 135.46, 136.93, 144.95, 157.77.

3-(1-(3-(dimethylamino)propyl)-4,5-diphenyl-1H-imidazol-2-yl)phenol (5f)

M.p. 194–196 °C; yield 90%. FT-IR (KBr, cm^{-1}): 3478 (OH), 3060, 3013 (C–H) aromatic, 2996–2722 (C–H) aliphatic, 1602 (C=N). ^1H NMR (DMSO- d_6 /D $_2$ O, 300 MHz): 1.42 (m., 2H, $\text{CH}_2\text{—CH}_2\text{—CH}_2$), 1.83 (s., 6H, $(\text{CH}_3)_2\text{N}$), 1.89 (t., 2H, $(\text{CH}_3)_2\text{NCH}_2\text{—CH}_2\text{—CH}_2\text{—N}$), 3.88 (t, 2H, $(\text{CH}_3)_2\text{NCH}_2\text{—CH}_2\text{—CH}_2\text{—N}$), 6.93–7.768 (m., 14H, Ar-H), 9.69 (s., 1H, Ar-OH). ^{13}C NMR (100 MHz, DMSO- d_6 /D $_2$ O): 28.31, 43.24, 45.02, 56.36, 115.86, 122.52, 126.51, 127.00, 128.16, 128.37, 129.15, 129.51, 129.61, 130.63, 131.41, 131.88, 135.45, 136.61, 147.53, 158.43.

4-(1-(3-(dimethylamino)propyl)-4,5-diphenyl-1H-imidazol-2-yl)-N,N-dimethyl aniline (5 g)

M.p. 147–149 °C; yield 88%. FT-IR (KBr, cm^{-1}): 3039, (C–H) aromatic, 2991–2711 (C–H) aliphatic, 1608 (C=N). ^1H NMR (DMSO- d_6 /D $_2$ O, 300 MHz): 1.42 (m., 2H, $\text{CH}_2\text{—CH}_2\text{—CH}_2$), 1.82 (s., 6H, $(\text{CH}_3)_2\text{NNCH}_2\text{—CH}_2\text{—CH}_2\text{—N}$), 1.88 (t., 2H, $(\text{CH}_3)_2\text{NCH}_2\text{—CH}_2\text{—CH}_2\text{—N}$), 2.98 (s., 6H, 4- $(\text{CH}_3)_2\text{N—Ph}$), 3.88 (t, 2H, $(\text{CH}_3)_2\text{NCH}_2\text{—CH}_2\text{—CH}_2\text{—N}$), 6.83–7.55 (m., 14H, Ar-H). ^{13}C NMR (100 MHz, DMSO- d_6 /D $_2$ O): 28.41, 43.29, 45.09, 45.56, 56.45, 112.33, 119.12, 126.26, 126.50, 128.36, 129.09, 129.95, 131.43, 131.99, 135.55, 136.64, 147.85, 150.90.

4-(1-(3-(dimethylamino)propyl)-4,5-diphenyl-1H-imidazol-2-yl)benzoic acid (5 h)

M.p. 176–178 °C; yield 94%. FT-IR (KBr, cm^{-1}): 3367 (OH), 3062 (C–H) aromatic, 2972–2952, 1669 (C=O) acidic, (C–H) aliphatic, 1586 (C=N). ^1H NMR (DMSO- d_6 /D $_2$ O, 300 MHz): 1.46 (m., 2H, $\text{CH}_2\text{—CH}_2\text{—CH}_2$), 1.88 (s., 6H, $(\text{CH}_3)_2\text{N}$), 1.97 (t., 2H, $(\text{CH}_3)_2\text{NCH}_2\text{—CH}_2\text{—CH}_2\text{—N}$), 3.99 (t, 2H, $(\text{CH}_3)_2\text{NCH}_2\text{—CH}_2\text{—CH}_2\text{—N}$), 4.77 (s., 1H, —COOH), 7.14–8.09 (m., 14H, Ar-H). ^{13}C NMR (100 MHz, DMSO- d_6 /D $_2$ O): 28.12, 43.44, 44.78, 44.94, 56.02, 126.60, 126.99, 128.94, 129.00, 129.44, 129.62, 129.97, 130.85, 131.39, 135.03, 137.49, 146.29, 167.71.

4-(1-(3-(dimethylamino)propyl)-4,5-diphenyl-1H-imidazol-2-yl)phenol (5i)

M.p. 240–241 °C; yield 91%. FT-IR (KBr, cm^{-1}): 3369 (OH), 3062 (C–H) aromatic, 2945–2667 (C–H) aliphatic, 1603 (C=N). ^1H NMR (DMSO- d_6 /D $_2$ O, 300 MHz): 1.39 (m., 2H, $\text{CH}_2\text{—CH}_2\text{—CH}_2$), 1.81 (s., 6H, $(\text{CH}_3)_2\text{N}$), 1.88 (t., 2H, $(\text{CH}_3)_2\text{NCH}_2\text{—CH}_2\text{—CH}_2\text{—N}$), 3.87 (t, 2H, $(\text{CH}_3)_2\text{NCH}_2\text{—CH}_2\text{—CH}_2\text{—N}$), 6.90–7.53 (m., 14H, Ar-H),

9.80 (s., 1H, OH). ^{13}C NMR (100 MHz, DMSO- d_6 /D $_2$ O): 28.25, 42.25, 45.07, 56.40, 115.85, 122.54, 126.22, 126.51, 128.28, 129.18, 129.52, 130.64, 131.41, 131.88, 135.450, 136.67, 147.51, 158.40.

3-(2-(4-methoxyphenyl)-4,5-diphenyl-1H-imidazol-1-yl)-N,N-dimethylpropan-1-amine (5j)

M.p. 86–88 °C; yield 86%. FT-IR (KBr, cm^{-1}): 3050–3017 (C–H) aromatic, 2966–2772 (C–H) aliphatic, 1602 (C=N). ^1H NMR (DMSO- d_6 /D $_2$ O, 100 MHz): 1.41 (m., 2H, $\text{CH}_2\text{—CH}_2\text{—CH}_2$), 1.79 (s., 6H, $(\text{CH}_3)_2\text{N}$), 1.87 (t., 2H, $(\text{CH}_3)_2\text{NCH}_2\text{—CH}_2\text{—CH}_2\text{—N}$), 3.83 (t, 2H, $(\text{CH}_3)_2\text{NCH}_2\text{—CH}_2\text{—CH}_2\text{—N}$), 3.90 (s., 3H, OCH $_3$), 7.10–8.12 (m., 14H, Ar-H). ^{13}C NMR (300 MHz, DMSO- d_6 /D $_2$ O): 28.35, 42.20, 45.05, 55.74, 56.36, 114.52, 124.18, 126.35, 126.55, 126.58, 128.16, 128.28, 129.18, 129.52, 129.89, 129.97, 130.62, 131.40, 131.81, 135.84, 136.88, 147.14, 160.13.

2-(1-(3-(dimethylamino)propyl)-4,5-diphenyl-1H-imidazol-2-yl)phenol (5 k)

M.p. 49–51 °C; yield 89%. FT-IR (KBr, cm^{-1}): 3460 (OH) phenolic, 3057–3026 (C–H) aromatic, 2957–2710 (C–H) aliphatic, 1599 (C=N). ^1H NMR (DMSO- d_6 /D $_2$ O, 300 MHz): 1.42 (m., 2H, $\text{CH}_2\text{—CH}_2\text{—CH}_2$), 1.82 (s., 6H, $(\text{CH}_3)_2\text{NNCH}_2\text{—CH}_2\text{—CH}_2\text{—N}$), 1.86 (t., 2H, $(\text{CH}_3)_2\text{NCH}_2\text{—CH}_2\text{—CH}_2\text{—N}$), 3.98 (t, 2H, $(\text{CH}_3)_2\text{NCH}_2\text{—CH}_2\text{—CH}_2\text{—N}$), 6.05 (s., 1H, OH), 7.12–7.79 (m., 14H, Ar-H). ^{13}C NMR (100 MHz, DMSO- d_6 /D $_2$ O): 28.25, 43.26, 45.02, 56.22, 115.98, 116.19, 126.19, 126.57, 128.15, 130.07, 131.57, 135.08, 136.95, 146.19, 161.55, 163.99.

5-(1-(3-(dimethylamino)propyl)-4,5-diphenyl-1H-imidazol-2-yl)-2-methoxy phenol (5 l)

M.p. 139–141 °C; yield 87%. FT-IR (KBr, cm^{-1}): 3361 (OH), 3055 (C–H) aromatic, 2991–2711 (C–H) aliphatic, 1607 (C=N). ^1H NMR (DMSO- d_6 /D $_2$ O, 300 MHz): 1.44 (m., 2H, $\text{CH}_2\text{—CH}_2\text{—CH}_2$), 1.82 (s., 6H, $(\text{CH}_3)_2\text{N}$), 1.88 (t., 2H, $(\text{CH}_3)_2\text{NCH}_2\text{—CH}_2\text{—CH}_2\text{—N}$), 3.85 (s., 3H, OCH $_3$), 3.90 (t, 2H, $(\text{CH}_3)_2\text{NCH}_2\text{—CH}_2\text{—CH}_2\text{—N}$), 7.04–7.52 (m., 13H, Ar-H), 9.04 (s, 1H, OH). ^{13}C NMR (300 MHz, DMSO- d_6 /D $_2$ O): 28.38, 43.27, 45.05, 56.20, 56.39, 112.69, 116.66, 120.26, 124.41, 126.39, 126.49, 128.42, 129.20, 129.54, 129.75, 131.42, 131.78, 135.36, 136.67, 147.03, 147.23, 148.77. DEPT 135 (100 MHz, DMSO- d_6): 28.38, 43.27, 56.39 (CH $_2$) ppm disappeared.

3-(2-(4-fluorophenyl)-4,5-diphenyl-1H-imidazol-1-yl)-N,N-dimethylpropan-1-amine (5 m)

M.p. 190–192 °C; yield 92%. FT-IR (KBr, cm^{-1}): 3049 (C–H) aromatic, 2937–2789 (C–H) aliphatic, 1600 (C=N). ^1H NMR (DMSO- d_6 /D $_2$ O, 300 MHz): 1.39 (m., 2H,

CH₂-CH₂-CH₂), 1.77 (s., 6H, (CH₃)₂N), 1.86 (t., 2H, (CH₃)₂NCH₂-CH₂-CH₂-N), 3.89 (t., 2H, (CH₃)₂NCH₂-CH₂-CH₂-N), 7.10–7.80 (m., 14H, Ar-H). ¹³C NMR (100 MHz, DMSO-*d*₆/D₂O): 28.25, 43.26, 45.02, 56.22, 115.98, 116.19, 126.19, 126.94, 128.15, 128.51, 129.22, 129.49, 130.15, 131.36, 131.49, 131.57, 135.08, 136.95, 146.19, 161.55, 163.99.

4-(1-(3-(dimethylamino)propyl)-4,5-diphenyl-1H-imidazol-2-yl)-2-methoxy phenol (5n)

M.p. 149–151 °C; yield 93%. FT-IR (KBr, cm⁻¹): 3361 (OH), 3055 (C–H) aromatic, 2991–2711 (C–H) aliphatic, 1607 (C=N). ¹H NMR (DMSO-*d*₆/D₂O, 300 MHz): 1.41 (m., 2H, CH₂-CH₂-CH₂), 1.81 (s., 6H, (CH₃)₂N), 1.90 (t., 2H, (CH₃)₂NCH₂-CH₂-CH₂-N), 3.85 (t., 2H, (CH₃)₂NCH₂-CH₂-CH₂-N), 3.91 (s., 3H, OCH₃), 6.91–7.93 (m., 13H, Ar-H), 9.41 (s, 1H, OH). ¹³C NMR (100 MHz, DMSO-*d*₆/D₂O): 28.33, 43.29, 45.01, 56.40, 113.89, 116.04, 122.22, 122.88, 126.37, 126.57, 127.01, 128.17, 128.39, 129.52, 129.89, 131.41, 131.84, 135.41, 135.88, 136.67, 147.53, 147.90, 148.09.

2.5 | *In vivo* anti-inflammatory activity

For the determination of the effects on acute inflammation, some of the synthesized compounds were screened for their *in vivo* anti-inflammatory activity using the carrageenan-induced paw oedema standard method.^[20–22] Adult albino rats weighing 130–170 g of both sexes (pregnant female animals were excluded) were divided into 11 groups each containing 6 animals. All rats were fasted overnight, then on the next day (day of experiment) each rat was hydrated uniformly by giving 3 ml of water orally to reduce the variability of oedema response. Before induction of inflammation by one hour, the test samples and indomethacin used as a reference were administered orally at doses of 100 and 10 mg kg⁻¹, respectively, as suspension in saline solution with the aid of a few drops of Tween 80. For the control group, saline solution containing a few drops of Tween 80 was taken orally. One hour after the oral administration of test samples and reference, each mouse was injected in the subplantar tissue of the right hind paw with 1% solution of carrageenan in saline (0.1 ml per rat). Before injection of carrageenan, the average volume (*V*₀) of the right hind paw of each rat was calculated from three readings that did not deviate more than 3%. The thickness of rat paw was measured at different time intervals, after 60, 120, 180, 240 and 300 min, with the aid of a digital micrometer (239–561–30-4099758, Mitoutoyo, Japan). The oedema was expressed as the difference between the thickness of injected and non-injected paws, and the percentage of inhibition for each rat and each group was obtained as follows:

$$\text{Percentage inhibition} = \frac{(V_t - V_o)_{\text{control}} - (V_t - V_o)_{\text{treated}}}{(V_t - V_o)_{\text{control}}} \times 100$$

where *V*_t represents the mean right paw thickness, *V*₀ represents the mean left paw thickness, (*V*_t - *V*₀)_{control} represents the mean increase in paw thickness in the control group of rats and (*V*_t - *V*₀)_{treated} represents the mean increase in paw thickness in rats treated with the tested compounds.^[23,24]

Data were collected, checked, revised and analysed. Quantitative variables from normal distribution were expressed as mean ± standard error (SE).

2.6 | Acute toxicity

The approximate LD₅₀ values for the highly active anti-inflammatory compounds **5f**, **5h** and **5i** were tested using male mice.^[18] Fifteen groups of mice each consisting of six animals were used. The compounds were given orally in doses of 10, 50, 100, 200 and 400 mg kg⁻¹, respectively. At 24 hours later, the percentage mortality in each group and for each compound was recorded. The LD₅₀ values were calculated using the method described by Litchfield and Wilcoxon.^[25]

2.7 | *In vitro* COX-1 and COX-2 inhibition test

The COX (ovine) inhibitor screening assay directly measures PGF_{2a} by SnCl₂ reduction of COX-derived PGH₂ produced in the COX reaction. The prostanoid product was quantified via enzyme immunoassay (EIA) using a broadly specific antiserum that binds to all the major PG compounds.

3 | RESULTS AND DISCUSSION

3.1 | Characterization of ZnFe₂O₄ nanoparticles

Characterization of the investigated ZnFe₂O₄ nanoparticles was done via SEM, FT-IR spectroscopy, VSM, EDS, thermogravimetric analysis (TGA/DTA/DTG), PXRD, TEM and high-resolution TEM (HRTEM).

3.1.1 | Structural characteristics for ZnFe₂O₄ nanoparticles

PXRD study of the prepared ZnFe₂O₄ nanoparticles confirmed the formation of single phase inverse spinel structure. We investigated the structure of the PXRD diffraction pattern (Figure 1). It is clear that no impurity peaks appear but the sample has polycrystalline pattern with face-centred cubic structure. Crystallite sizes of ZnFe₂O₄ were estimated using Sherrer's formula.^[2–4,26–28]

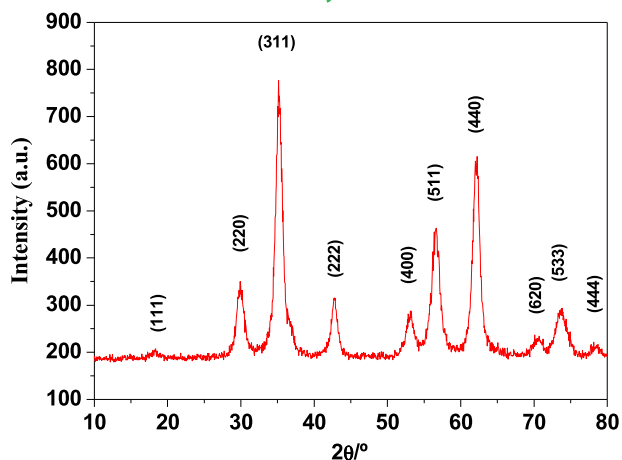


FIGURE 1 PXRD pattern for the prepared ZnFe_2O_4 nanoparticles

$$D = \frac{0.89\lambda}{\beta \cos \theta}$$

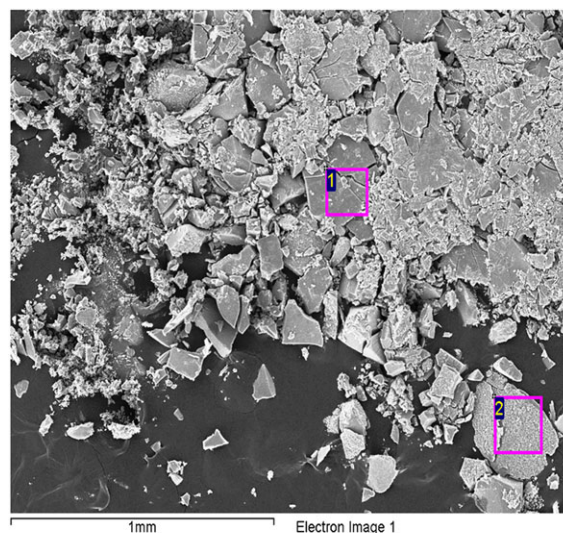
where β is the angular line width at half maximum intensity and θ is the Bragg angle for the actual peak. Maximum intensity peak (311) was used to estimate the crystallite size and it is found to be 10 nm in accordance with TEM estimation. All diffraction peaks can be indexed to the phase of ZnFe_2O_4 material, which match well with the standard data file of bulk cubicspinel-structured ZnFe_2O_4 (JCPDS 22–1012).^[29]

3.1.2 | FT-IR spectra of ZnFe_2O_4 nanoparticles

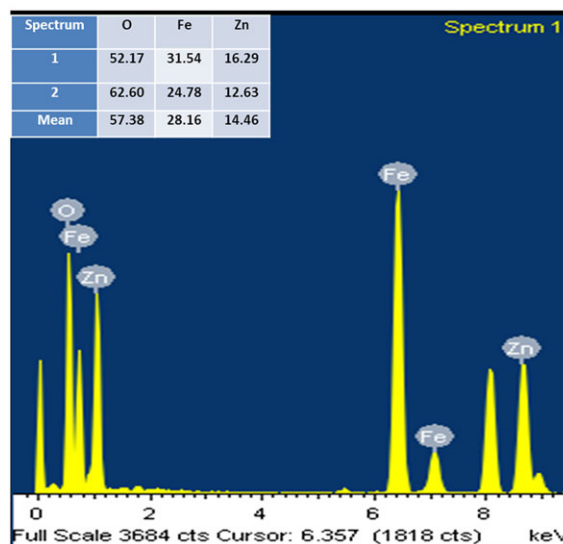
Figure S1 shows the FT-IR spectra taken from the samples. Two main broad metal–oxygen bands are seen in the FT-IR spectra of all spinels, and ferrites in particular. The highest one (Fig. S15) generally observed in the range $550\text{--}600\text{ cm}^{-1}$ corresponds to intrinsic stretching vibrations of the metal at the tetrahedral site, $\text{M}_{\text{tetra}}\text{--O}$, whereas the second highest band, usually observed in the range $385\text{--}450\text{ cm}^{-1}$, is assigned to octahedral metal stretching, $\text{M}_{\text{octa}}\text{--O}$.^[30] It is known that Zn^{2+} ions preferentially occupy octahedral sites, while Fe^{3+} ions can occupy both octahedral and tetrahedral sites.^[31] However, no clear peak due to octahedrally coordinated metal ions has been observed which is expected to be below 400 cm^{-1} . Since our FT-IR spectra ranges between 400 and 4000 cm^{-1} , we could not observe octahedral metal stretching, $\text{M}_{\text{octa}}\text{--O}$, which is attributed to a lower band. This may be due to the broadening of this peak attributed to very small particles of spinel ferrites.^[32]

3.1.3 | SEM and TEM

Qualitative analysis, via SEM-EDS, was used to obtain line scans (an example of which is presented in Figure 2b as well as area scans in Figure 2a), which reveal that ZnFe_2O_4 was



(a)



(b)

FIGURE 2 SEM-EDS analysis of the prepared ZnFe_2O_4 nanoparticles

successfully prepared with a homogenous and uniform distribution, while the results of quantitative analysis are confirmed by EDS (depicted Figure 2b). The morphology of the ZnFe_2O_4 nanoparticles was estimated via SEM (Figure 3). Uniformly dispersed spherical particles are observed, along with weak agglomerations. TEM image (Figure 4a) of ZnFe_2O_4 sample shows uniform distribution of nearly spherical particles, with an average size of $10 (\pm 2)$ nm (Figure 5), which is consistent with the value calculated from PXRD measurements. The HRTEM image displayed in Figure 4(b) for the prepared ZnFe_2O_4 sample proves the high crystallinity of these nanoparticles with interplanar spacings of 4.8 \AA corresponding to (111), (220) and (311) atomic planes of Zn–ferrite phase. Selected area

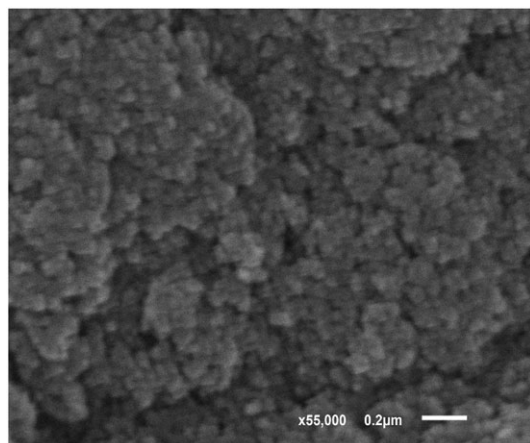


FIGURE 3 SEM image of the prepared ZnFe_2O_4 nanoparticles

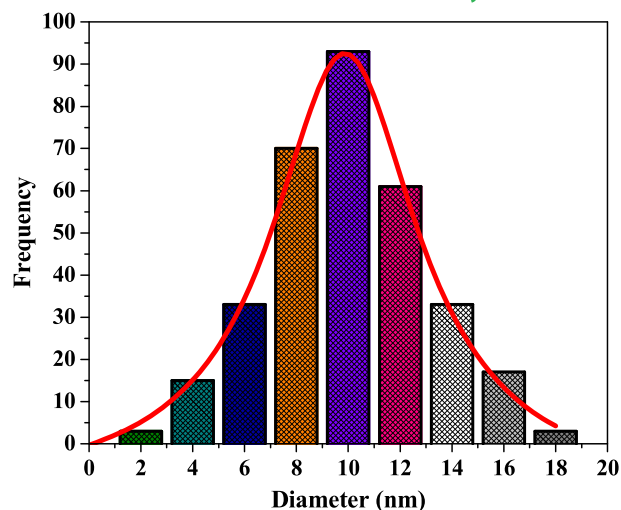
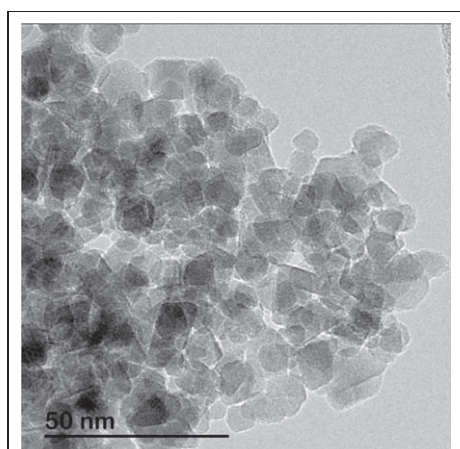
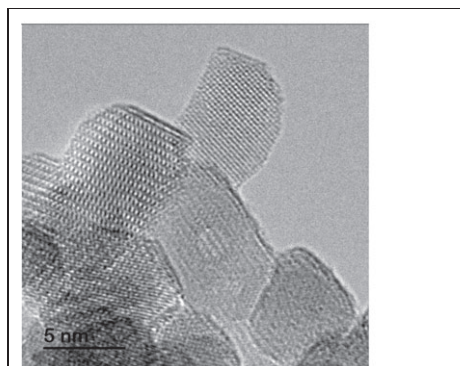


FIGURE 5 Particle size distribution for the prepared ZnFe_2O_4 nanoparticles



(a) Low magnification TEM image of the prepared ZnFe_2O_4 nanoparticles



(b) HRTEM image of the prepared ZnFe_2O_4 nanoparticles

FIGURE 4 (a) low-magnification TEM and (b) HRTEM images of the prepared ZnFe_2O_4 nanoparticles

electron diffraction (SAED) pattern (Figure 6) showed the polycrystalline nature of the samples and all the rings have been indexed as cubic spinel ZnFe_2O_4 phase. Moreover, SAED and PXRD patterns are found to agree that the (311)

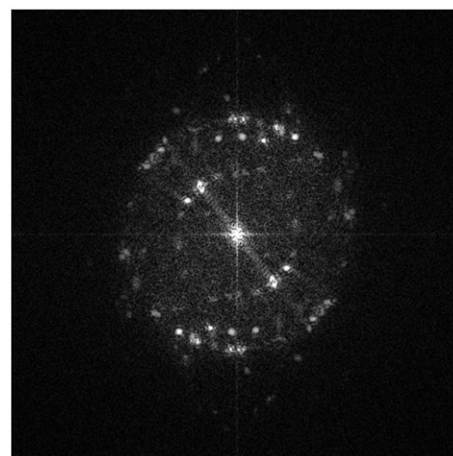


FIGURE 6 SAED pattern of the prepared ZnFe_2O_4 nanoparticles

plane showed the most intense reflection. The nanometric size of the prepared ZnFe_2O_4 particles results in a high surface area and this can lead to many interesting catalytic and other potential properties.^[33–35]

3.1.4 | TGA of ZnFe_2O_4 nanoparticles

The thermal stability of the prepared ZnFe_2O_4 nanoparticles in air was investigated. The TG/DTG curves are shown in Fig. S16. In the TG/DTG curves for ZnFe_2O_4 , the mass loss proceeds in four steps with total mass loss of *ca* 7.53%. The first and second steps are continuous with mass loss of *ca* 4.22% between 25 and 220 °C (which reach their maximum rate at 90 and 185 °C), which are attributed to the vaporization of surface and trapped water molecules. The third and fourth steps between 240 and 620 °C (which reach their maximum rate at 320 and 545 °C) with mass loss of *ca* 3.31%

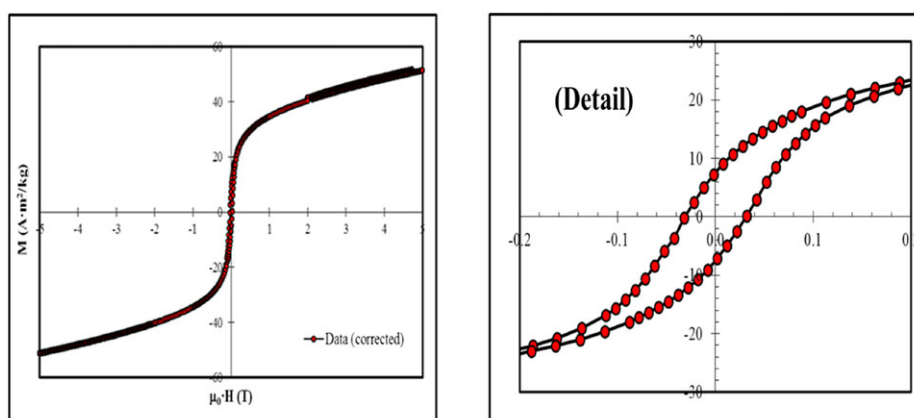
may be due to the loss of organic moiety. Thus, the catalyst is stable up to 220 °C, confirming that it could be safely used in organic reactions at temperatures in the region of 80 °C.

3.1.5 | Magnetic characterization

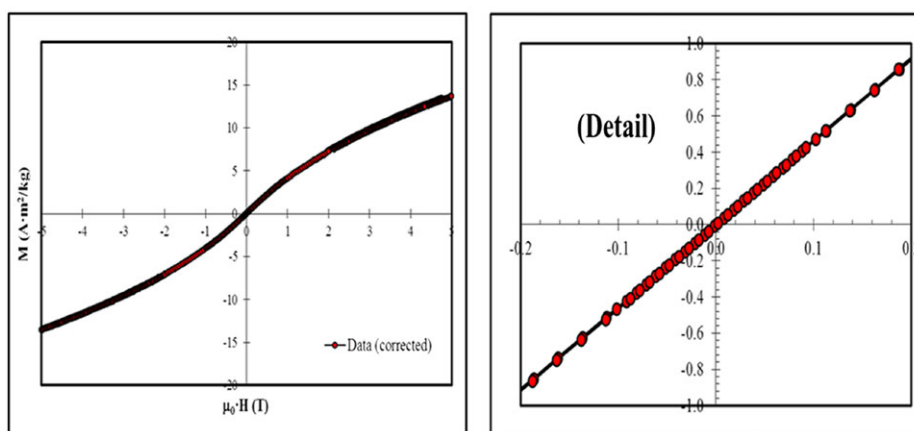
Figure 7(a) shows the curve of magnetization versus applied field (M - H loops) measured at 5 K for the prepared ZnFe_2O_4 . These loops show hysteretic behaviour with a significant coercively H_C and retentively M_R (see detail in Figure 7a). Meanwhile, saturation M_S is not reached even under the maximum field measured up to 50 kOe. Even so, the values of M_S have been calculated fitting the high field region (above 20 kOe) by means of the following approach-to-saturation law: $M = M_S(1 - b/H^2) + \chi_{\text{HF}}H$,^[36] with b being a constant related to crystal anisotropy and χ_{HF} the forced susceptibility. Table 1 includes all of these magnetic parameters that are

consistent with ferrimagnetic ordering accompanied by spin canting contribution. In this way, the saturation magnetization of spinel ferrites originates from the difference in the magnetic moments of the cations occupying the octahedral lattice sites and those located in the tetrahedral sites. As Zn^{2+} cation is not magnetic ($0 \mu_B$), its value for Zn ferrites directly reflects the distribution of the Fe^{3+} ions ($5 \mu_B$) between the two sub-lattices and therefore it is determined by inversion parameter δ . Moreover, competing interactions result into some degree of frustration that it is favoured for atoms at the nanoparticle surface, where broken magnetic exchange bonds are more common, yielding to spin canting^[37] that involves the large χ_{HF} measured.

At higher temperatures, the thermal energy overcomes the energy barrier so this causes the particle magnetization to rotate freely resulting in the absence of magnetism at zero applied magnetic field (superparamagnetic state). In this



(a) Magnetic field dependence of the magnetization measured at 5 K (M - H) and its detail



(b) Magnetic field dependence of the magnetization measured at 300 K (M - H) and its detail

FIGURE 7 Magnetic field dependence of magnetization (a) measured at 5 K (M - H) and its detail and (b) measured at 300 K (M - H) and its detail

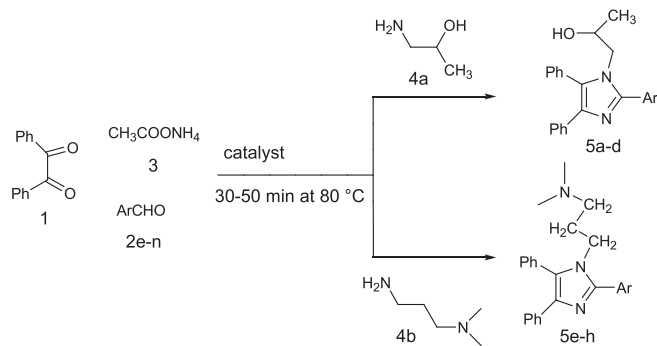
TABLE 1 Magnetic parameters for the prepared ZnFe_2O_4 magnetic nanoparticles

T_B (K)	H_C , 5 K (Oe)	M_R , 5 K (emu mol^{-1})	M_S , 5 K (emu mol^{-1})	B , 5 K (kOe^2)	χ_{HF} , 5 K ($\text{emu mol}^{-1}\cdot\text{kOe}^{-1}$)
25(1)	310(5)	1820(20)	8800(20)	25.7(6)	73.2(3)

way, magnetization versus applied field loops measured at 300 K show that there is no hysteresis (see Figure 7b) confirming the superparamagnetism for the prepared ZnFe₂O₄ nanoparticles.

3.2 | ZnFe₂O₄ magnetic nanoparticles for synthesis of multi-substituted imidazoles

On the basis of an exhaustive literature review, it has been found that 1,2,4,5-tetrasubstituted imidazoles have good biological activity. So, it was decided to study the application of the ZnFe₂O₄ nanoparticle catalyst for the synthesis of multi-substituted 1,2,4,5-tetrasubstituted imidazoles **5a–n** in excellent yields, as a simple, mild, expeditious and environmentally friendly method. Benzil (**1**), aromatic aldehydes (**2a–k**) and ammonium acetate (**3**) were reacted with 1-amine-2-propanol (**4a**) or *N,N*-dimethyl-3-aminopropane (**4b**) with ZnFe₂O₄ magnetic nanoparticles under solvent-free conditions (Scheme 1; Table 2). All the new compounds were



SCHEME 1 Synthesis of 1,2,4,5-tetrasubstituted imidazoles **5a–n**

investigated with FT-IR and NMR analyses (Section 1 and Figures S1–S14).

Initially, we explored and optimized various reaction parameters for the synthesis of the investigated compounds. The best results are obtained in the presence of 5 mmol% ZnFe₂O₄ nanoparticles at 80 °C in EtOH which give excellent yields of products compared with **5a*** in the absence of catalyst (Table 2).

The highest yield of product in the shortest time was obtained using ZnFe₂O₄ magnetic nanoparticles which may be due to their greater diffusion in the reaction mixture.

The results illustrate that the reactions proceed well with electron-withdrawing and electron-donating aromatic aldehydes.

With the optimized reaction conditions in hand, we investigated the model reaction further by varying the amount of the ZnFe₂O₄ magnetic nanoparticles. It was observed that 5 mmol% gave the highest yield of 96% and further increase were not beneficial to the process (Table 3).

To understand the role of Zn in the present catalytic system, two independent reactions with 6 mmol% nano-Fe₃O₄ and ZnFe₂O₄ catalysts were carried out under the optimized reaction conditions. As evident from Table 4, lower yield is observed with nano-Fe₃O₄, clearly indicating that Zn is the active catalytic centre in this reaction. An increase in yield (Table 4) with ZnFe₂O₄ nanoparticles shows that Fe plays a constructive role, possibly in the re-oxidation of Zn during the catalytic cycle.^[3,4,38]

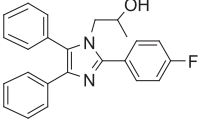
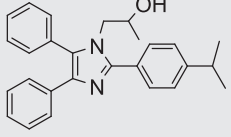
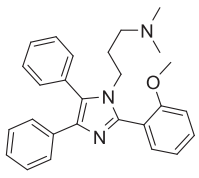
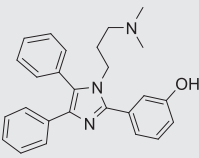
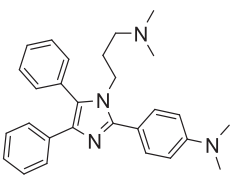
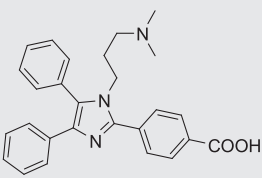
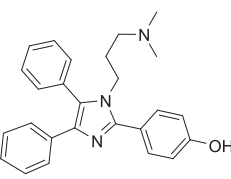
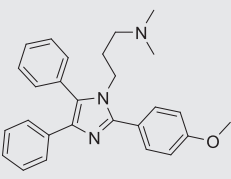
Solvents represent a major factor of the environmental performance of processes in the chemical industry and also have an impact on safety, cost and health issues. The idea of 'green' solvents expresses the goal of minimizing the envi-

TABLE 2 ZnFe₂O₄ magnetic nanoparticles as catalyst for synthesis of multi-substituted imidazoles **5a–n**

Compound	Ar	Formula (mol. Wt)	Structure	M.p. (°C)	Time (min)	Yield (%)
5a*	2-HOPh	C ₂₄ H ₂₂ N ₂ O ₂ (370.17)		80–82	55	25
5a	2-HOPh	C ₂₄ H ₂₂ N ₂ O ₂ (370.17)		80–82	55	87
5b	4-HOPh	C ₂₄ H ₂₂ N ₂ O ₂ (370.17)		212–214	35	88

(Continues)

TABLE 2 (Continued)

Compound	Ar	Formula (mol. Wt)	Structure	M.p. (°C)	Time (min)	Yield (%)
5c	4-FPh	C ₂₄ H ₂₁ FN ₂ O (372.43)		170–172	25	96
5d	4-isopropyl-Ph	C ₂₇ H ₂₈ N ₂ O (396.52)		198–200	30	92
5e	2-CH ₃ OPh	C ₂₇ H ₂₉ N ₃ O (411.55)		121–123	60	92
5f	3-HOPh	C ₂₆ H ₂₇ N ₃ O(397.52)		194–196	50	90
5 g	4-(CH ₃) ₂ NPh	C ₂₈ H ₃₂ N ₄ (424.26)		147–149	55	88
5 h	4-HOOCPh	C ₂₇ H ₂₇ N ₃ O ₂ (425.53)		176–178	43	94
5i	4-HOPh	C ₂₆ H ₂₇ N ₃ O (397.52)		240–241	40	91
5j	4-CH ₃ OPh	C ₂₇ H ₂₉ N ₃ O (411.55)		86–88	55	86

(Continues)

TABLE 2 (Continued)

Compound	Ar	Formula (mol. Wt)	Structure	M.p. (°C)	Time (min)	Yield (%)
5 k	2-HOPh	C ₂₆ H ₂₇ N ₃ O (397.52)		49–51	60	89
5 l	3-HO-4-CH ₃ Oph	C ₂₇ H ₂₉ N ₃ O ₂ (427.55)		139–141	57	87
5 m	4-FPh	C ₂₆ H ₂₆ FN ₃ (399.51)		190–192	50	92
5n	4-HO-3-CH ₃ Oph	C ₂₇ H ₂₉ N ₃ O ₂ (427.55)		149–151	60	93

TABLE 3 Amount of ZnFe₂O₄ catalyst for synthesis of multi-substituted imidazole 5c^a

Entry	Catalyst (mmol%)	Yield (%) ^b	Entry	Catalyst (mmol%)	Yield (%) ^b
1	1	30	5	4	84
2	2	44	6	5	96
3	3	57	7	6	96

^aReaction conditions: **1** (1 mmol), **2a** (1 mmol), **3** (1 mmol), **4** (1 mmol).^bIsolated yield based on **5c**.TABLE 4 Reaction yield in presence of Fe₃O₄ and ZnFe₂O₄ catalysts

Entry	Catalyst	Tim (min)	Yield (%)
1	Fe ₃ O ₄ nanoparticles	30	80
2	ZnFe ₂ O ₄ nanoparticles	30	96

ronmental impact resulting from the use of solvents in chemical production. We used various solvents such as ethanol, methanol, DMSO, CHCl₃, MeCN and toluene under similar reaction conditions. The maximum obtained yield was in EtOH (Table 5).

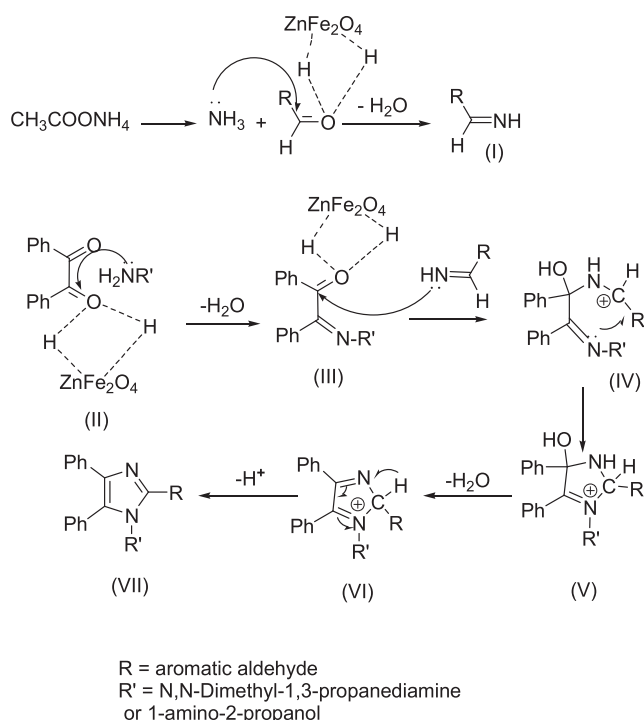
TABLE 5 Effect of solvent on the synthesis of multi-substituted imidazole 5c using ZnFe₂O₄ nanoparticles^a

Solvent	Time (min)	Yield (%) ^b
Toluene	190	60
CHCl ₃	180	63
DMSO	160	71
EtOH	35	96
MeOH	90	87

^aReaction conditions: **1** (1 mmol), **2a** (1 mmol), **3** (1 mmol), **4** (1 mmol) and 5 mmol% catalyst.^bIsolated yield based on **5c**.

The possible mechanism of the four-component cyclocondensation of benzil, aliphatic amine (**4a** or **4b**) and the appropriate aromatic aldehyde together with ZnFe_2O_4 magnetic nanoparticles in the presence of ammonium acetate includes a key coupling step of the intermediate of the benzaldehyde imine (I) to the activated catalytic iminobenzil (III) of aliphatic amine (**4a** or **4b**) followed by cyclization giving the corresponding 1,2,4,5-tetrasubstituted imidazoles (Scheme 2).

Reusability is another very favourable property of the catalyst under investigation. The reusability of the catalyst was evaluated under the reaction conditions described above for the model reaction. After completion of the



SCHEME 2 Possible mechanism of synthesis of multi-substituted imidazoles **5a–n**

reaction, the catalyst is easily recovered by applying a strong external permanent magnet, followed by washing with ethanol to remove the residual product(s), drying under vacuum, and reusing directly for the next cycle without further treatment (Scheme 3). The catalyst can be used for five runs, and no obvious loss in catalytic activity is observed (Figure 8).

The catalyst was investigated after reuse of five times using SEM (Fig. S17). SEM images of the nanoparticles before and after the reaction show identical shapes. Therefore, it can be concluded that the morphology of the nanoparticles remains unchanged after reaction. Finally, the recovered catalyst was subjected to TEM analysis (Figure 9a) and the change in size was found to be negligible (11 nm; Figure 9b).

3.3 | *In vivo* anti-inflammatory activity

The anti-inflammatory activity of nine of the synthesized compounds was determined by using the standard method

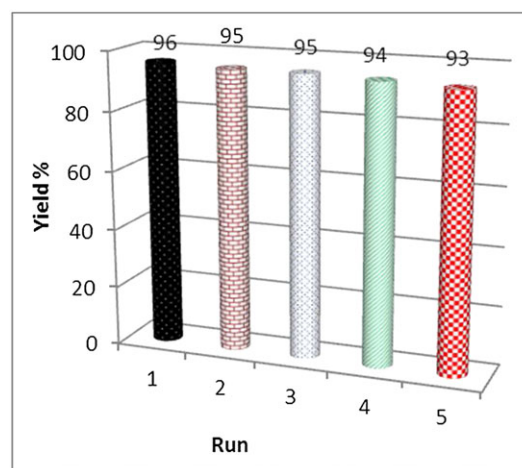


FIGURE 8 Recyclability of ZnFe_2O_4 magnetic nanoparticles in the model reaction for synthesis of 1,2,4,5-tetrasubstituted imidazoles



SCHEME 3 Separation of catalyst (ZnFe_2O_4) from reaction mixture using an external magnet

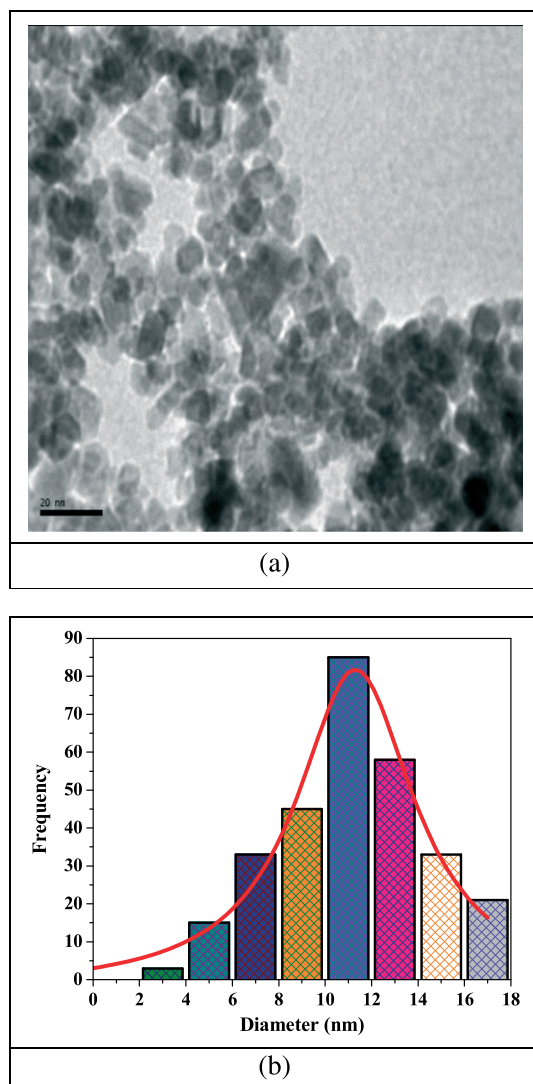


FIGURE 9 (a) TEM image of prepared ZnFe_2O_4 nanoparticles after catalytic reaction. (b) particle size distribution of recovered ZnFe_2O_4 nanoparticles

of carrageenan-induced paw oedema in rats. It is observed from the obtained results (Tables 6 and 7; Figure 10) that all the tested compounds show considerable anti-inflammatory activity compared with that of the reference standard indomethacin (85.8% inhibition of oedema). In addition, it is clear from Tables 6 and 7 that **5 h**, **5 f** and **5 i** exhibit the highest anti-inflammatory activity, with maximum activity in the case of **5 h**, followed by **5 f** and **5 i** (94.66 to 91.28% inhibition of oedema).

Comparing the activity of 2-hydroxypropylimidazole derivatives we found that **5 c** and **5 d** show high to moderate anti-inflammatory activity compared with the reference standard indomethacin. On the other hand, by comparing the anti-inflammatory activity of all the synthesized compounds, it is found that substitution by the electron-withdrawing

TABLE 7 Anti-inflammatory activity of tested compounds using carrageenan-induced paw oedema in rats

Compound	Inhibition of oedema (%)				
	1 h	2 h	3 h	4 h	5 h
Control	0	0	0	0	0
Indomethacin	40.55	53.73	54.56	85.8	60.37
5 c	8.93	13.87	62.17	85.83	82.99
5 d	2.61	21.12	48.49	76.57	71.19
5 e	10.49	14.18	20.43	44.35	5.24
5 f	9.22	23	65.11	91.28	73.17
5 g	20.44	23.08	53.87	63.53	78.39
5 h	30.89	66.72	81.045	94.66	86.45
5 i	26.65	47.85	87.94	93.3	79.19
5 j	38.32	46.79	63.18	81.7	71.22
5 k	27.04	37.22	50.74	77.43	78.63

TABLE 6 Percentage of oedema of the tested compounds using carrageenan-induced paw oedema in rats

Compound	Oedema (mean \pm SE) (%)					
	0 h	1 h	2 h	3 h	4 h	5 h
Control	27.67 \pm 1.92	30.52 \pm 2.58	33.19 \pm 2.57	36.85 \pm 1.11	38.5 \pm 1.1	44.16 \pm 0.99
Indomethacin	13.87 \pm 0.52	19.73 \pm 1.81	10.89 \pm 1.24	17.05 \pm 0.48	5.46 \pm 1.48	17.5 \pm 1.48
5 c	17.87 \pm 0.17	30.23 \pm 0.33	26.28 \pm 0.33	13.94 \pm 1.29	5.46 \pm 1.68	7.51 \pm 2.26
5 d	20.85 \pm 1.23	32.32 \pm 1.58	24.07 \pm 1.9	18.98 \pm 3.04	9.02 \pm 3.64	12.72 \pm 5.2
5 e	18.18 \pm 1.29	32.98 \pm 1.02	28.48 \pm 1.14	24.28 \pm 1.38	21.42 \pm 0.71	41.85 \pm 1.85
5 f	16.62 \pm 1.79	30.13 \pm 1.34	23.5 \pm 2.54	12.86 \pm 1.79	3.36 \pm 2.17	11.85 \pm 2.01
5 g	15.66 \pm 1.58	26.41 \pm 1.46	23.47 \pm 1.58	17.00 \pm 1.26	14.04 \pm 1.73	9.54 \pm 4.55
5 h	20.13 \pm 0.78	21.09 \pm 3.91	11.05 \pm 1.78	6.99 \pm 2.079	2.06 \pm 0.38	5.98 \pm 1.47
5 i	16.08 \pm 1.75	24.34 \pm 0.5	15.91 \pm 0.75	4.44 \pm 0.68	2.58 \pm 0.44	9.19 \pm 0.89
5 j	24.23 \pm 1.45	18.82 \pm 2.33	17.66 \pm 1.69	13.57 \pm 1.64	7.05 \pm 1.54	12.71 \pm 3.77
5 k	18.72 \pm 3.38	26.89 \pm 6.93	20.84 \pm 0.69	15.03 \pm 1.064	8.69 \pm 1.22	9.44 \pm 1.92

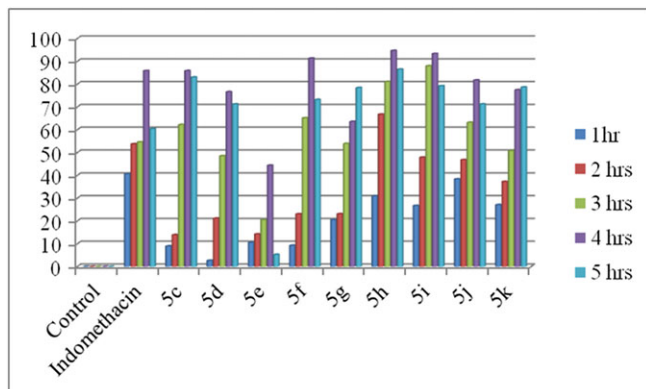


FIGURE 10 Percentage inhibition of oedema of the tested compounds

(COOH) group as in compound **5 h** leads to a marked increase in potency compared with the electron-donating basic (CH_3)₂N group as in compound **5c**.

By comparing the biological activity of the present synthesized compounds with those reported in the literature,^[39] we found that compound **5c** which contains the 2-(4-fluorophenyl)imidazole moiety shows higher activity than compound **5c** which contains the 2-(4-chlorophenyl)imidazole moiety. This may be due to the higher electronegativity of fluoride atom at *para* position than chloride atom. Also, the newly synthesized compounds **5 h** and **5i** containing the 1-(*N*-dimethylaminopropyl)imidazole moiety show more potent activity than compound **5d**^[39] which has the isopropanol moiety instead. Moreover, compound **5f** has a high biological activity which is attributed to the presence of a hydroxyl group in *meta* and *para* positions.

3.4 | *In vitro* COX-1 and COX-2 inhibition test

The COX (ovine) inhibitor screening assay directly estimates PGF_{2a} by SnCl₂ reduction of COX-derived PGH₂ produced in the COX reaction. The prostanoid product is quantified via EIA using a broadly specific antiserum that connects to all the major PG compounds.

This assay involves both ovine COX-1 and human recombinant COX-2 enzymes allowing the user to screen isozyme-specific inhibitors. This assay is a pre-eminent tool that can be used for general inhibitor screening, or to eliminate false positive leads generated by less specific methods.

The ability of the test compounds to inhibit ovine COX-1 and human recombinant COX-2 (IC₅₀ value, 1 M) was determined using an EIA kit (catalogue no. 560131, Cayman Chemical, Ann Arbor, MI, USA) according to a previously reported method.^[40]

Upon using the *in vitro* COX-1 and COX-2 inhibition test, it was observed from the obtained results (Table 8) that all the tested compounds showed considerable anti-

TABLE 8 *In vitro* COX-1, COX-2 inhibition, anti-inflammatory activity of tetrasubstituted imidazoles **5c–5 k** and reference drugs celecoxib, diclofenac sodium and indomethacin

Compound	COX-1 IC ₅₀ (μm)	COX-2 IC ₅₀ (μm)	COX-2 SI ^a (μm)
Celecoxib	14.8	0.05	296
Diclofenac sodium	3.9	0.8	4.88
Indomethacin	0.039	0.49	0.080
5c	12.4	0.19	65.26
5e	8.9	0.41	21.71
5f	10.6	0.14	75.71
5 g	10.5	0.39	26.92
5 h	13.4	0.11	121.82
5i	12.7	0.12	105.83
5j	11.4	0.19	60.00
5 k	9.4	0.24	39.17

^aCyclooxygenase-2 specific inhibitors.

inflammatory activity compared with the three standards celecoxib, diclofenac sodium and indomethacin. Also, from the results in Table 8 it is clear that dimethylaminopropylimidazole derivatives **5 h**, **5i** and **5f** exhibited the highest anti-inflammatory activity with COX-2 SI (cyclooxygenase-2 specific inhibitors) activities of 121.82, 105.83 and 75.71, respectively.

4 | CONCLUSIONS

ZnFe₂O₄ magnetic nanoparticles were synthesized hydrothermally and characterized via various physicochemical techniques. Moreover, the prepared ZnFe₂O₄ magnetic nanoparticles were used as an environmentally friendly heterogeneous catalyst for the synthesis of 14 new compounds of imidazols derivatives. This protocol has some advantages of excellent to high yields, highly pure products, enhanced rapid reaction rates and short reaction times, compatibility with different functional groups, simplicity of operation and easy work-up. Also, ZnFe₂O₄ magnetic nanoparticles are an available, cheap, stable, reusable and environmentally acceptable catalyst. Hence, we believe that this method will find wide application in organic synthesis as well as industry. Also the imidazole derivatives showed potent anti-inflammatory action compared with reference standard indomethacin. The dimethylaminopropylimidazole derivatives showed the greatest activity beginning with **5 h**, then **5f** and to **5i**. Also, the presence of (COOH) group as an electron-withdrawing group (**5 h**) in the *para* position resulted in a greater potency

than the presence of basic $(\text{CH}_3)_2\text{N}$ group as an electron-withdrawing one.

REFERENCES

- [1] K. Layek, H. Maheswaran, M. L. Kantam, *Catal. Sci. Technol.* **2013**, *3*, 1147.
- [2] M. Abd El Aleem Ali El-Remaily, A. M. Abu-Dief, *Tetrahedron* **2015**, *71*, 2579.
- [3] A. M. Abu-Dief, I. F. Nassar, W. H. Elsayed, *Appl. Organometal. Chem.* **2016**, *30*, 917.
- [4] M. Abd El Aleem Ali El-Remaily, A. M. Abu-Dief, R. M. El-Khatib, *Appl. Organometal. Chem.* **2016**, *30*, 1022.
- [5] L. Yu, M. Wang, P. Li, L. Wang, *Appl. Organometal. Chem.* **2012**, *26*, 576.
- [6] S. B. Simonsen, D. Chakraborty, I. Chroendorff, S. Dahl, *Appl. Catal. A* **2012**, *447–448*, 22.
- [7] A. M. Abu-Dief, S. K. Hamdan, *Am. J. Nano Sci.* **2016**, *2*, 26.
- [8] Q. Zhang, H. Su, J. Luo, Y. Wei, *Catal. Sci. Technol.* **2013**, *3*, 235.
- [9] M. A. A. El Remaily, *Tetrahedron* **2014**, *70*, 2971.
- [10] W. Yang, J. Li, J. Li, Q. Chen, G. Yang, *Bioorg. Med. Chem. Lett.* **2012**, *22*, 1455.
- [11] L. H. Abdel-Rahman, A. M. Abu-Dief, N. M. Ismaila, M. Ismael, *Inorg. Nano-Metal Chem.* **2017**, *47*, 467.
- [12] M. Petrusov, H. Smrticov, B. Pribulov, S. Vlckov, I. Uhliarikov, T. Docsa, A. Somsak, L. Petru, *Tetrahedron* **2016**, *72*, 2116.
- [13] H. Zetty Zulikha, R. A. Haque, S. Budagumpi, A. M. S. Abdul Majid, *Inorg. Chim. Acta* **2014**, *411*, 40.
- [14] S. Pusch, T. Opatz, *Org. Lett.* **2014**, *16*, 5430.
- [15] B. Sammaiah, D. Sumalatha, S. Reddy, M. Rajeswari, L. Sharada, *Int. J. Ind. Chem.* **2012**, *3*, 11.
- [16] M. Bahnous, A. Bouraiou, M. Chelghoum, S. Bouacida, T. Roisnel, F. Smati, C. Bentchouala, P. Gros, A. Belfaitah, *Bioorg. Med. Chem. Lett.* **2013**, *23*, 1274.
- [17] W. Liu, W. Guo, J. Wu, Q. Luo, F. Tao, Y. Gu, Y. Shen, J. L. R. Tan, Q. Xu, Y. Sun, *Biochem. Pharm.* **2013**, *85*, 1504.
- [18] M. Pieczonka, A. Strzelczyk, B. Sadowska, G. Mlosto, P. Staczek, *Eur. J. Med. Chem.* **2013**, *64*, 389.
- [19] F. Malihe, M. Hosseini, H. Kiani, *J. Saudi Chem. Soc.* **2016**, *20*, S503.
- [20] L. H. Abdel-Rahman, A. M. Abu-Dief, E. F. Newair, S. Kamel Hamdan, *J. Photochem. Photobiol. B* **2016**, *160*, 18.
- [21] E. Pintado, F. X. Malcata, J. E. Carvalho, *Mar. Drugs* **2010**, *8*, 1763.
- [22] S. M. El-Moghazy, F. F. Barsoum, H. M. Abdel-Rahman, A. A. Marzouk, *Med. Chem. Res.* **2012**, *21*, 1722.
- [23] M. E. Shoman, M. Abdel-Aziz, O. M. Aly, H. H. Farag, M. A. Morsy, *Eur. J. Med. Chem.* **2009**, *44*, 3068.
- [24] E. M. N. Abdel-Hafez, G. E. A. A. Abu-Rahma, M. Abdel-Aziz, M. F. Radwan, H. H. Farag, *Bioorg. Med. Chem.* **2009**, *17*, 3829.
- [25] M. Spetea, C. R. Bohotin, M. F. Asim, K. Stübbegger, H. Schmidhammer, *Eur. J. Pharm. Sci.* **2010**, *41*, 125.
- [26] L. H. Abdel-Rahman, A. M. Abu-Dief, R. M. El-Khatib, S. M. Abdel-Fatah, *J. Photochem. Photobiol. B* **2016**, *162*, 298.
- [27] L. H. Abdel-Rahman, A. M. Abu-Dief, R. M. El-Khatib, S. M. Abdel-Fatah, *Bioorg. Chem.* **2016**, *69*, 140.
- [28] E. M. M. Ibrahim, A. M. Abu-Dief, A. Elshafaie, A. M. Ahmed, *Mater. Chem. Phys.* **2017**, *192*, 41.
- [29] J. Q. Wan, X. H. Jiang, H. Li, K. Z. Chen, *J. Mater. Chem.* **2012**, *22*, 13500.
- [30] S. Hafner, *Z. Kristallogr.* **1961**, *115*, 331.
- [31] P. P. Hankare, V. T. Vader, N. M. Patil, S. D. Jadhav, U. B. Sankpal, M. R. Kadam, B. K. Chougule, N. S. Gajbhiye, *Mater. Chem. Phys.* **2009**, *113*, 233.
- [32] M. Sertkol, Y. Köseoğlu, A. Baykal, H. Kavas, M. S. Toprak, *J. Magn. Magn. Mater.* **2010**, *322*, 866.
- [33] L. H. Abdel Rahman, A. M. Abu-Dief, N. A. Hashem, A. A. Seleem, *Int. J. Nanomater. Chem.* **2015**, *1*, 79.
- [34] L. H. Abdel Rahman, A. M. Abu-Dief, S. K. Hamdan, *Catal. Lett.* **2016**, *146*, 1373.
- [35] L. H. Abdel Rahman, A. M. Abu-Dief, S. K. Hamdan, A. A. Seleem, *Int. J. Nanomater. Chem.* **2015**, *1*, 65.
- [36] A. M. Abu-Dief, M. S. M. Abdelbaky, D. Martínez-Blanco, Z. Amghouz, S. García-Granda, *Mater. Chem. Phys.* **2016**, *174*, 164.
- [37] C. Yao, Q. Zeng, G. F. Goya, T. Torres, J. Liu, H. Wu, M. Ge, Y. Zeng, Y. Wang, J. Z. Jiang, *J. Phys. Chem. C* **2007**, *111*, 12274.
- [38] M. Abd El Aleem Ali El-Remaily, H. A. Hamad, *J. Mol. Catal. A* **2015**, *404*, 148.
- [39] A. A. Marzouk, A. A. Abdelhamid, S. K. Mohamed, J. Simpson, *Z. Naturforsch. B* **2017**, *72*, 23.
- [40] B. Roschek, R. C. Fink, D. Li, M. McMichael, C. M. Tower, R. D. Smith, R. Alberte, *J. Med. Food* **2009**, *12*, 615.

SUPPORTING INFORMATION

Additional Supporting Information may be found online in the supporting information tab for this article.

How to cite this article: Marzouk AA, Abu-Dief AM, Abdelhamid AA. Hydrothermal preparation and characterization of ZnFe_2O_4 magnetic nanoparticles as an efficient heterogeneous catalyst for the synthesis of multi-substituted imidazoles and study of their anti-inflammatory activity. *Appl Organometal Chem.* 2017; e3794. <https://doi.org/10.1002/aoc.3794>